PNAS RESEARCH ARTICLE | ENGINEERING

A standing Leidenfrost drop with Sufi whirling

Jinlong Yang[a,1], Yong Li[a,b,1], Dehui Wang[a,1], Yue Fan[c], Yuanyuan Ma[a], Fanfei Yu[a], Junchang Guo[a], Longquan Chen[d], Zuankai Wang[e], and Xu Deng[a,f,2]

Edited by Manoj K. Chaudhury, Lehigh University, Bethlehem, PA; received April 6, 2023; accepted July 1, 2023 by Editorial Board Member Pablo G. Debenedetti

When a water drop is placed on a hot solid surface, it either undergoes explosive contact boiling or exhibits a stable state. In the latter case, the drop floats over an insulating layer of vapor generated by rapid vaporization of water at the surface/drop interface; this is known as the Leidenfrost state. Here, we discuss a previously unrecognized steady state in which a water drop "stands" on a hot smooth surface. In this state, the drop stabilizes itself with partial adhesion on the hot surface, leading to unique deformation and rotation behavior reminiscent of Sufi whirling—a form of spinning dance. Our analysis of this standing Leidenfrost state reveals the underlying mechanisms that drive the drop's stable partial adhesion and subsequent deformation with rotation. The heat-transfer efficiency of this standing state is up to 390% greater than that of the traditional floating Leidenfrost state.

Leidenfrost state | drop | wettability

Significance

It is commonly believed that a Leidenfrost drop remains stable by floating over a self-vaporized cushion, which suppresses heat transfer. Here, we revealed a stable Leidenfrost state with partial adhesion so that the water drops "stand" on a hot smooth surface. The "standing" state exhibited markedly more efficient heat transfer than the conventional "floating" state. In this standing Leidenfrost state, the drop further evolves to deform horizontally and rotates in a similar manner to Sufi whirling. We have unveiled the evolution of the standing Leidenfrost state and the driving mechanism of the deformation and rotation.

The classic boiling process, which is characterized by the onset of nucleate boiling, transition boiling, and film boiling in sequence with increasing surface temperature, is widely used in various industrial processes (1–5). Both nucleate boiling and transition boiling exist in an unstable state, which is characterized by violent disturbances at the substrate/water interface. During film boiling, when a sufficiently high temperature is reached, the substrate/water interface is replaced by a thin vapor layer, which makes the boiling mild and stable. For a drop on a hot surface, this stable state is known as the Leidenfrost state (6), in which the drop entirely floats above a thin vapor layer (7, 8). This thin vapor layer makes the drop highly mobile, leading to various dynamic behaviors, such as oscillation (9–11), transportation (12–16), and bouncing (17–21). It is widely believed that a highly unstable transition state with a narrow temperature gap exists on hydrophilic surfaces before the Leidenfrost state forms. This state is characterized by repeated nucleation and bursting of bubbles (7) (see the description of the boiling process in *SI Appendix*, Fig. S1 and Note S1).

In contrast to the classic boiling regimes described above, we observed an additional stable state in which the drop "stands" on a heated hydrophobic surface with partial adhesion to the surface, which we refer to as a standing Leidenfrost state. In this state, the drop further evolves into a horizontally deformed shape and rotates like a Sufi whirling dervish (Movie S1). In this study, we explore the physical mechanisms underlying the stable partial adhesion and self-rotation.

Results and Discussion

Standing Leidenfrost State with Sufi Whirling. The standing Leidenfrost state was studied by placing a water drop on a hot sapphire slide that was chemically and topologically homogeneous, as illustrated in Fig. 1*A*. The experimental setup is shown in *SI Appendix*, Fig. S2*A*, and atomic force microscopy (AFM) images of the surface are shown in *SI Appendix*, Fig. S2*B*. The surface was grafted with poly(dimethylsiloxane) (PDMS-Cl) molecules (22) to render it hydrophobic. The apparent water contact angle was 110° ± 2° with a contact-angle hysteresis of 23° ± 1° at room temperature (Fig. 1*B*). We observed the transformation of a water drop on this substrate using a high-speed camera and analyzed the sequential drop profiles. As the temperature was increased, the water drop began to boil, which is known as nucleate and transition boiling (Fig. 1*B*). Upon a further increase in temperature, the drop underwent short-term violent boiling before settling into a Leidenfrost state. However, unlike the typical Leidenfrost state (7, 23), in which the drop entirely hovers over an insulating vapor layer (Fig. 1*D*), this type of standing drop was observed when the substrate was heated to approximately 170 °C (Fig. 1*C*). In this state, the vapor layer coexisted with partial adhesion of the liquid to the substrate, causing the drop to appear as if it were "standing" on the surface supported by "feet".

Held by the vapor cushion around the "feet," the drop was found to deform into an ellipsoid-like shape (Fig. 1*E* and Movie S1). Specifically, the 20-μL ellipsoidal drop rotated

Author affiliations: [a]Institute of Fundamental and Frontier Sciences, University of Electronic Science and Technology of China, Chengdu 610054, China; [b]Digital Media Art Key Laboratory of Sichuan Province, Sichuan Conservatory of Music, Chengdu 610021, China; [c]School of Materials Science and Engineering, Sun Yat-sen University, Guangzhou 510275, China; [d]School of Physics, University of Electronic Science and Technology of China, Chengdu 610054, China; [e]Department of Mechanical Engineering, The Hong Kong Polytechnic University, Hong Kong 999077, China; and [f]Shenzhen Institute for Advanced Study, University of Electronic Science and Technology of China, Shenzhen 518110, China

Author contributions: J.Y., Y.L., D.W., and X.D. designed research; J.Y., Y.F., and Y.M. performed research; F.Y. and J.G. contributed new reagents/analytic tools; J.Y., Y.L., D.W., L.C., Z.W., and X.D. analyzed data; and J.Y., D.W., Z.W., and X.D. wrote the paper.

The authors declare no competing interest.

This article is a PNAS Direct Submission. M.K.C. is a guest editor invited by the Editorial Board.

[1]J.Y., Y.L. and D.W. contributed equally to this work.

[2]To whom correspondence may be addressed. Email: dengxu@uestc.edu.cn.

This article contains supporting information online at https://www.pnas.org/lookup/suppl/doi:10.1073/pnas.2305567120/-/DCSupplemental.

Published August 1, 2023.

with a period of approximately 23 ms. We designated the equatorial and polar radii of the drop as L and D, respectively. The turning angle, which was defined by the rotation of the long axis from the horizontal line, was designated as φ. Fig. 1*F* shows a plot of φ and the aspect ratio L/D during rotation (the full lifespan of the standing Leidenfrost drop can be seen in Movie S2 and *SI Appendix*, Fig. S3). The linear variation of φ indicates that the drop rotated at a constant angular speed, and the L/D ratio was nearly constant, revealing that the drop maintained a steady shape. Under the conditions used for this demonstration, the drop rotated at a constant frequency of approximately 43 Hz. By analyzing the aspect ratio throughout the drop's lifespan (*SI Appendix*, Fig. S3 and Movie S2), we found that the aspect ratio evolved from a value close to one (i.e., a spherical shape) to a value close to 1.6 (i.e., an ellipsoidal shape) before decaying with a decrease in drop volume. Fig. 1 *G* and *H* depict the probability of standing Leidenfrost state on smooth hydrophobic sapphire slides, illustrating the effects of varying drop volume and substrate temperature on the standing state. It was observed that the standing Leidenfrost state exhibited a specific range of drop volume and temperature. When the drop volume was small, it tended to adopt a spherical shape with minimal contact with the surface. The formation of feet was infrequent due to the limited contact area and surface tension constraints. In the case of a large-volume drop, the presence of a substantial central vapor blister rendered the drop unstable and caused the feet to easily vanish. The boiling state of the drop was directly influenced by the surface temperature. At low surface temperatures, the evaporation of the drop did not generate enough vapor to sustain stable feet, resulting in unstable boiling. Conversely, at high temperatures, the drop rapidly evaporated and entered a floating Leidenfrost state. The hydrophobicity of the surface impacted the boiling state on a smooth surface as well. A stable standing Leidenfrost state was exclusively observed on smooth hydrophobic surfaces, while no stable state was observed until reaching the floating Leidenfrost state for hydrophilic surfaces.

Origin of the Rotation in the Standing Leidenfrost State. We reexamined the evolution of L/D and the angular velocity, ω_o, during rotation (*SI Appendix*, Fig. S3). Despite changes in L/D, which indicate variations in the drop shape, ω_o remained constant from the start of the rotation. The constant angular velocity led us to hypothesize that the deformation and rotation are not propelled by outer forces but are triggered by inner circulation. We used particle image velocimetry (PIV) to visualize the flow field of the drop at the central horizontal plane (1 mm from the bottom)—an approach similar to those taken in the literature (12, 24, 25). As shown in Fig. 2*A* and Movie S3, inner circulation occurred before the deformation of the drop into an ellipsoidal shape. The inner angular velocity, ω_i, was determined from the flow field. The results, which are plotted in Fig. 2*B*, reveal a gradual increase in the circulation prior to the asymmetric deformation of the drop. ω_i reached 130 rad/s for a drop with added fluorescent particles, which is consistent with ω_o. Subsequently, the symmetric flow led to asymmetric deformation of the drop (Movie S3).

We used the Weber number ($We = \rho\omega_o^2 R^3/\gamma$) to examine the influence of the centrifugal force and the surface tension on the standing Leidenfrost drop, where ρ is the density of the water, R is the radius of the drop before deformation, and γ is the surface

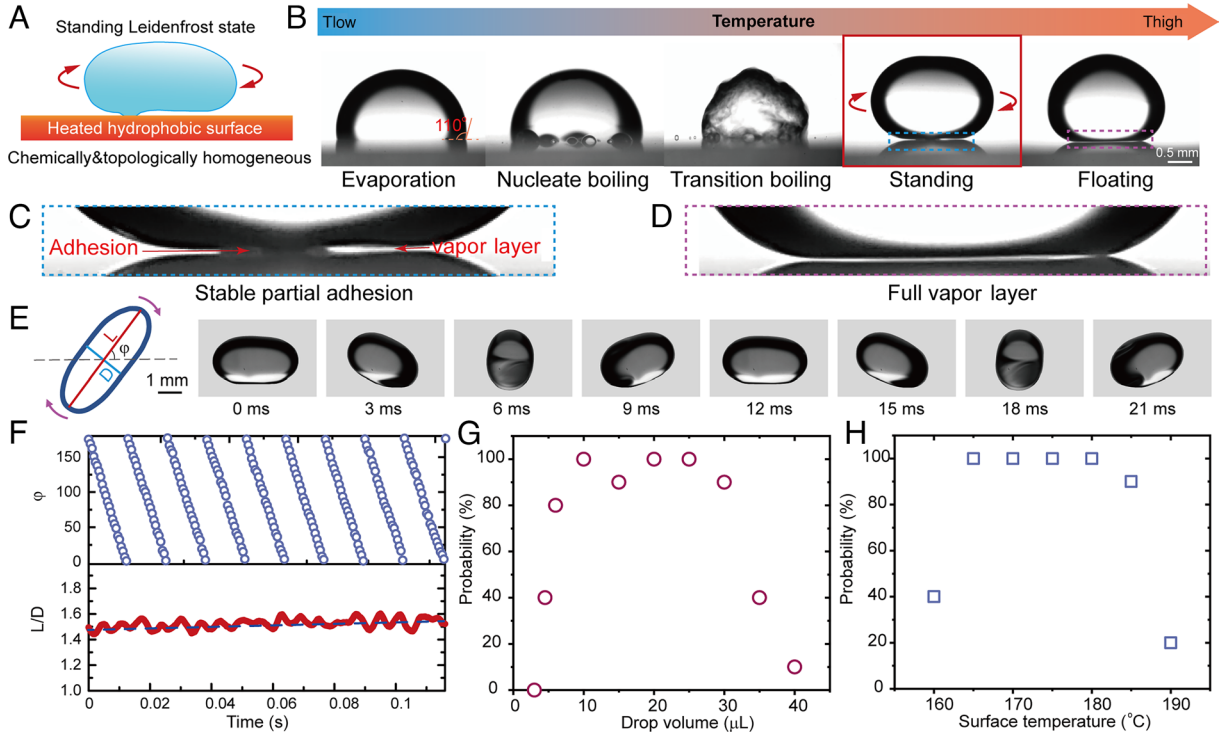

Fig. 1. Standing Leidenfrost state followed by rotation similar to Sufi whirling. (*A*) Schematic illustration of the standing Leidenfrost state and the experimental conditions. A water drop is gently deposited on a heated hydrophobic slide that is chemically and topologically homogeneous. The drop then self-adjusts its adhesion on the surface and further deforms and rotates. (*B*) Water drops (20 μL) on the hydrophobic sapphire slide with increasing temperature. In addition to the conventional floating Leidenfrost state with a full vapor layer, a stable standing Leidenfrost state with partial adhesion is observed. In this state, the drop may undergo horizontal deformation and rotate in a similar manner to Sufi whirling. (*C*) Partial adhesion in the standing state. (*D*) Full vapor layer in the floating state. (*E*) A single rotation period of a standing Leidenfrost drop. The 20-μL drop deforms into an ellipsoidal shape and rotates with a typical period of 23 ms. (*F*) Variation in the turning angle, φ, and the aspect ratio, L/D, over five periods for a rotating drop with a volume of 20 μL. φ, L, and D are defined in (*E*). (*G* and *H*) The probability of standing Leidenfrost state on smooth hydrophobic sapphire slides as a function of drop volume (*G*) and surface temperature (*H*). The probability is measured by at least 10 drops in different places.

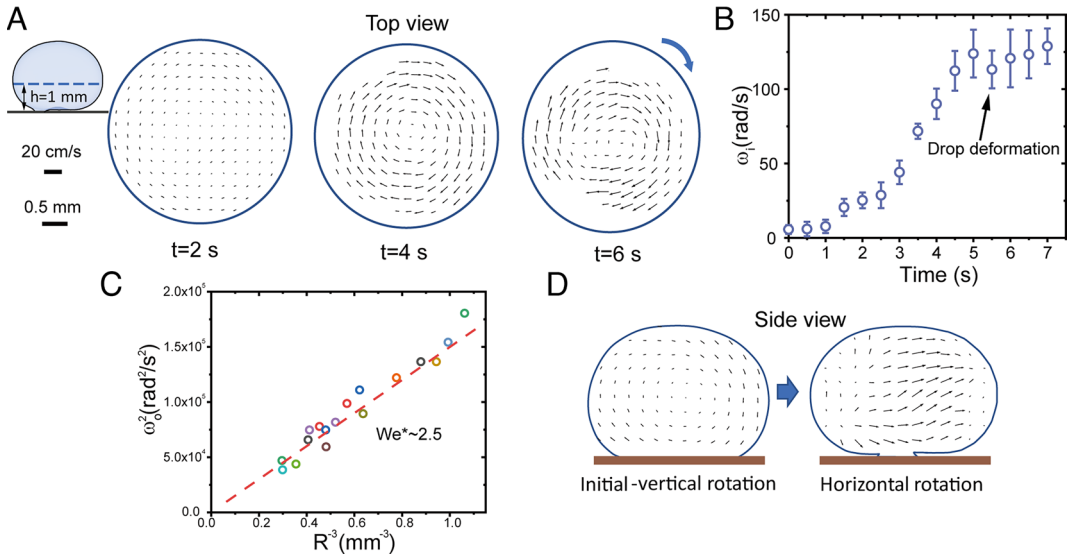

Fig. 2. Origin of the deformation and rotation of drops in the standing Leidenfrost state. (*A*) Evolution of the inner flow at the horizontal central plane (1 mm from the bottom) captured by PIV measurements. Tracer particles reveal that circulation first occurs inside the drop before deformation of the drop into an ellipsoidal shape. (*B*) Inner rotating velocity, ω_i, as a function of time. ω_i increases from an initial value of zero to a critical value when the drop deforms into an ellipsoidal shape. The drop remains spherical despite the inner circulation during the increasing period. (*C*) Linear relation between ω_o and the size of the drop. (*D*) Evolution of the inner flow at the vertical central plane. Vertical circulation finally evolves to horizontal circulation inside the drop in the standing Leidenfrost state.

tension of the water. *We* was approximately unity, indicating that both the momentum and the surface tension play significant roles prior to deformation. With increasing *We*, the centrifugal force surpassed the cohesive force, rendering the drop susceptible to small vibrations that induced a break in symmetry at a critical *We* (*We**). From our experimental conditions with varying drop radii (*R*), *We** was calculated to be ~2.5 (Fig. 2*C*). Notably, this value corresponds to the critical dimensionless angular velocity ($\omega^* = (We^*/8)^{1/2} \sim 0.56$) reported in the literature (26–28), despite the different drop sizes used in the experiments. At values above *We**, the drop became unstable, with vibrations causing deformation and the conversion of kinetic energy into surface energy, resulting in elongation of the drop. Under our experimental conditions, this break in symmetry led to the formation of ellipsoid shapes belonging to the two-lobed shape family. This behavior was anticipated given the small *We**. During rotation, the dissipation of kinetic energy and the reduction in the volume due to evaporation eventually rendered the momentum insufficient to sustain the drop's shape. As a result, surface tension caused the drop to revert to a sphere (Movie S2 and *SI Appendix*, Fig. S3). The rotation of a freestanding drop driven by inner circular flow has been the subject of long-standing interest because it is related to various phenomena, ranging from atomic nuclear fission to planetary rotation. Experimental and theoretical investigations have been undertaken to elucidate the underlying mechanisms and progression of drop rotation and asymmetric deformation (26–31). Methods have been developed to trigger the rotation of the drop since the pioneering experiments conducted by Plateau (26, 28–30). Our findings demonstrated that self-rotation inside the drop can be initiated in a standing Leidenfrost drop.

Origin of the Inner Circulation in the Standing Leidenfrost State. Drop rotation was triggered by inner circulation. Therefore, we now examine how the horizontal circulation begins inside the drop. Previous studies on the inner circulation of floating Leidenfrost drops focused on the vertical direction (12, 32), with circulation stimulated by the symmetry shear force from vapor ejection at the bottom of the drop. Drops hovering entirely over a vapor layer may have either vertical counterrotative convective cells or a single rotating cell, depending on the drop size (12). For drops with partial adhesion, by imaging the vertical central plane (Fig. 2*D*) and the horizontal plane at h = 0.5 mm using PIV (*SI Appendix*, Fig. S4*A*), we observed a transition from vertical to horizontal circulation. According to the Poincaré–Brouwer theorem, in the case of shear-induced surface flow, there is guaranteed to be at least one stationary point with zero value on the sphere (33). Accordingly, a horizontal gradient or shear force is exerted on the drop, leading to circulation within the drop, and the stationary point is typically located at the top of the drop. We attributed the inner horizontal circulation to partial adhesion, which affects both the thermal and mechanical properties of the drop. Partial adhesion enhances heat transfer from the "feet". This accelerates the evaporation, which induces high shear flow underneath the drop. The asymmetric heat flow from the bottom also breaks the vertical heat-gradient-driven flow. For a drop with an aspect ratio (*2R/H*) greater than unity, the constraint for single-cell circulation in the horizontal direction is weaker than that in the vertical direction. Here, *H* is the height of the drop. The circulation shifts from the vertical to the horizontal plane. Partial adhesion also changes the direction of airflow underneath the drop, thus breaking the symmetry of the outflow of air from the center. This results in the development of a tangential flow that drives the horizontal circulation inside the drop. A numerical simulation confirmed that the circulation at the bottom of the drop rapidly initiates the inner circulation of the entire drop (*SI Appendix*, Fig. S4*B*).

We further explored how the partial adhesion influences the airflow that drives the inner circulation of the drop in the standing Leidenfrost state. Because the drop is held by the elevated vapor pressure, a concave shape develops at its bottom. Adhesion areas frequently occurred at the periphery of the air cushion, resulting in shear flow along the outer edge. This shifted the vertical circulation to the horizontal direction, ultimately leading to horizontal circulation inside the drop. Upon surpassing a critical angular velocity, this horizontal circulation stimulated the rotation of the drop. We verified this process of airflow-induced horizontal circulation using an air-blowing device (Movie S4).

Partial Adhesion in the Standing Leidenfrost State. To understand the mechanism responsible for the formation of this stable state, we monitored the changes in the contact area at the interface beneath the drop using a high-speed camera (as illustrated in the Fig. 3 *A*, *Inset*). Fig. 3*A* and Movie S5 depict the liquid–solid contact area of the adhesion region of a 20-μL water drop that was gently deposited on a transparent hydrophobic sapphire slide as a function of time. The dashed line in Fig. 3*A* represents the change in surface temperature at the bottom and center of the deposited drop (Movie S6). The inset images show the adhesion during the evolution of the contact area, with the black region indicating the site of adhesion. The contact region rapidly vibrated after the initial deposition of a water drop on the surface but quickly stabilized within 1 s. The process of adhesion was observed to include five distinct stages. Upon contact of the water drop with the hot hydrophobic surface, immediate bubble generation was observed, indicating that nucleate boiling occurred until full contact with the surface was achieved (stage I). The bubbles then grew and merged, resulting in a slight reduction in the contact area (stage II). The increase in the liquid–solid contact area and the subsequent nucleate boiling resulted in a significant dissipation of heat from the substrate. The surface temperature consequently decreased rapidly. Mild boiling was observed during these two stages (Movie S5). When the temperature recovered, the bubbles merged to form a partial vapor film, which occupied most of the area underneath the drop (stage III). The increased vapor pressure, which was constrained by the surface tension, then resulted in the formation of a dimple of vapor at the bottom of the drop (stage IV). When the vapor occupied the majority of the drop bottom, stable feet formed. The feet were generated at the periphery of this dimple, which was expected because the periphery is closest to the surface and the formation of feet helps stabilize the drop on the vapor cushion. The drop was observed to "stand" on the surface with several feet around the underlying vapor layer. However, this was not the final state because the vapor accumulated with limited leakage among the feet. The feet self-adjusted their number and size to balance the vapor pressure and gravity, resulting in a stable standing Leidenfrost drop with partial adhesion (stage V). Once standing, the drop continued to deform and rotate (Movie S5).

We then analyzed the underlying factors that drive the evolution of drop–surface interactions. Fig. 3*A* illustrates the evolution of the contact area, indicating successive interactions between the drop and the hot surface, from nucleate boiling to transition boiling and finally stable partial film boiling.This progression prompted us to examine the role of the surface temperature. When the drop touched the hot surface, the heat-transfer process between the drop and the hot surface was transient and mainly governed by the ratio of convective heat transfer in the drop to conductive heat transfer within the substrate (34) (as shown in the *Inset* of *SI Appendix*, Fig. S5 and Note S2). We utilized Biot number [$Bi = L_c/\lambda/(1/h)$] to quantify this ratio in transient heat transfer. Here, $1/h$ is the thermal resistance of convective heat transfer, with h being the coefficient of surface heat transfer at boiling. L_c/λ is the thermal resistance of conductive heat transfer, where L_c denotes the characteristic length, and λ refers to the coefficient of conductivity. In the specific scenario where a drop is placed on slides, L_c corresponds to the thickness of the slides. For a water drop boiling on a sapphire slide with a thickness of 2 mm, Bi is on the order of unity, indicating that the surface temperature falls between the temperature of the drop and the substrate. We used the thermal effusivity ($e = (\lambda \rho c_p)^{1/2}$) to describe the ability of the materials to exchange thermal energy with their surroundings, where ρ is

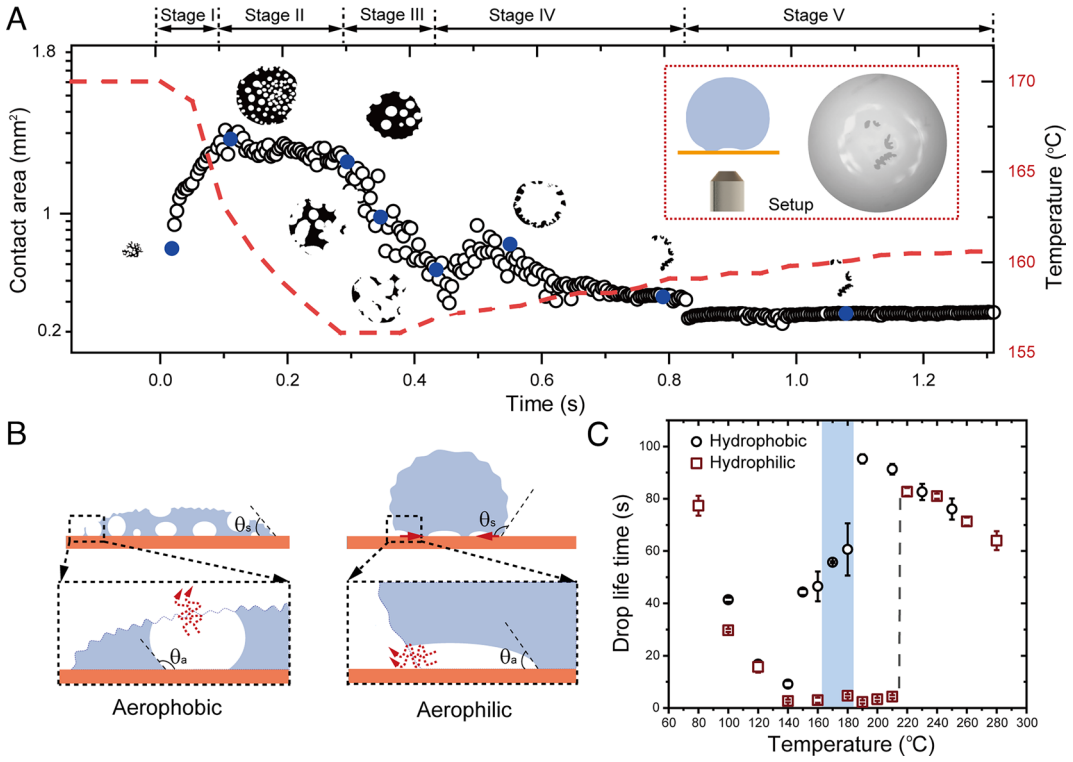

Fig. 3. Origin of the stable standing Leidenfrost state with partial adhesion. (*A*) Evolution of the contact area (black circles) and surface temperature (red dotted line) for a standing Leidenfrost drop on a hydrophobic sapphire plate with the temperature set at 170 °C. The *Inset* shows the experimental setup used to observe the evolution of the drop/surface interface, and sequential images of the adhesion are shown above the data in the graph (corresponding to the blue dots). (*B*) Schematic depiction of the influence of wettability on boiling. (*C*) Lifetime of a drop with a volume of 20 μL placed on hydrophobic and hydrophilic sapphire slides. The shaded area represents the range of substrate temperatures at which the standing Leidenfrost state was observed.

the density, and c_p is the specific heat capacity (35, 36). For a water drop and substrate with initial temperatures of T_w and T_s, respectively, the temperature at the contact surface, T_i, can be determined from their relative effusivities as follows:

$$T_i = T_w + \frac{e_s}{e_s + e_w}(T_s - T_w), \quad [1]$$

where e_s and e_w are the effusivities of the substrate and water, respectively. For a low e_s/e_w ratio, T_i is close to the water temperature, whereas for a high ratio, it is close to the substrate temperature. As shown in *SI Appendix*, Fig. S5, the change in surface temperature is governed by the e_s/e_w ratio, displaying a decrease followed by a slow recovery only when the ratio was within a certain range. This evolution of surface temperature enabled the drop to regulate its adhesion to the surface and reach thermal equilibrium (the boiling of a water drop on different hot substrates is demonstrated in Movie S7). Conventionally, for the Leidenfrost state on substrates with high e_s/e_w ratios, the initial contact is assumed to be instantaneous and is thus neglected (7). In this scenario, the rapid recovery of T_i leads to the fast evaporation of the drop at the bottom such that the drop enters the Leidenfrost state with a fully formed vapor layer. Conversely, when the surface temperature was insufficient for rapid evaporation, the drop either made full contact or underwent violent boiling in an unstable manner (as shown in Movie S7). By tracking the state of the drop on substrates with different e_s/e_w ratios, a Leidenfrost state with stable partial adhesion was generally observed for moderate ratios of thermal effusivity (as shown in *SI Appendix*, Fig. S6 and Table S1).

The hydrophobicity (or aerophilicity) of the surface further enhanced the ability of the drop to "stand up". The hydrophobicity has a dual impact on the boiling process. First, the surface energy determines the morphology of the deposited drop (37), as shown in Fig. 3*B*. On hydrophobic surfaces, a reduction in the contact area leads to a lower heat transfer from the surface to the drop. Second, nucleating bubbles on a hydrophobic (aerophilic) surface merge and escape at the apparent contact line without compromising the integrity of the drop. The reduced contact area and heat transfer enable the drop to reach a stable state. By contrast, on hydrophilic (aerophobic) surfaces, nucleating bubbles burst at the air/liquid interface, making the drop highly unstable. To confirm the role of hydrophobicity on the partial adhesion in the standing Leidenfrost state, we examined the behavior of drops on heated fluorinated surfaces (rather than PDMS) with the same degree of hydrophobicity (apparent water contact angle of 112° ± 2° and contact-angle hysteresis of 23° ± 1° at room temperature). The drops exhibited a comparable change of contact area on both surfaces (*SI Appendix*, Fig. S7). Fig. 3*C* shows the drop lifetime as a function of the substrate temperature. In comparison to the sharp increase in drop lifetime observed during the transition from contact boiling to film boiling on a hydrophilic smooth substrate, the lifetime of a drop on a hydrophobic smooth surface exhibited a distinct step-like behavior with an increase in surface temperature. The drop's lifetime was primarily determined by the heat flux it received. The notable disparity in conductivity between the liquid phase (680 mW/m·°C) and the vapor phase (24.8 mW/m·°C) underscored the crucial role played by the connection between the drop and the surface in determining its lifetime. In the case of a floating Leidenfrost drop, where the drop was fully surrounded by vapor, there was a significant reduction in heat flux, leading to a considerable increase in lifetime. On the other hand, for a standing Leidenfrost drop, where vapor predominantly occupied the bottom portion of the drop, the heat flux to the drop was limited, resulting in a noticeable extension of its lifetime. However, the small adhesion presenting in the standing state may still provide a pathway for rapid heat flux, thereby resulting in a reduction of lifetime compared to the floating Leidenfrost state.

Finally, we demonstrated the control of drop motion due to the enhanced heat transfer in the standing Leidenfrost state. The analysis of the equilibrium state for standing Leidenfrost drops prompted us to explore the use of asymmetric substrates with distinct thermal effusivity to control drop rotation (*SI Appendix*, Figs. S8 and S9 and Note S3). By patterning materials with low e_s on a substrate with high e_s, we demonstrated controllable drop rotation (Fig. 4*A* and Movie S8) and sustained rotation with constant drop size and frequency (Fig. 4*B* and Movie S9). Owing to the partial adhesion on the surface in the standing Leidenfrost state (with 15% adhesion), there was noticeably higher (by 390%) heat flow from the substrate to the drop than in the conventional floating Leidenfrost state (Fig. 4 *C* and *D* and *SI Appendix*, Note S4).

In summary, our findings reveal a stable standing Leidenfrost state in which a water drop is partially adhered to a hot smooth surface, rather than completely hovering over a vapor layer. We analyzed the origin of this standing state, taking into consideration the surface temperature, hydrophobicity, and the equilibrium of this state. Furthermore, we demonstrated how this partial adhesion

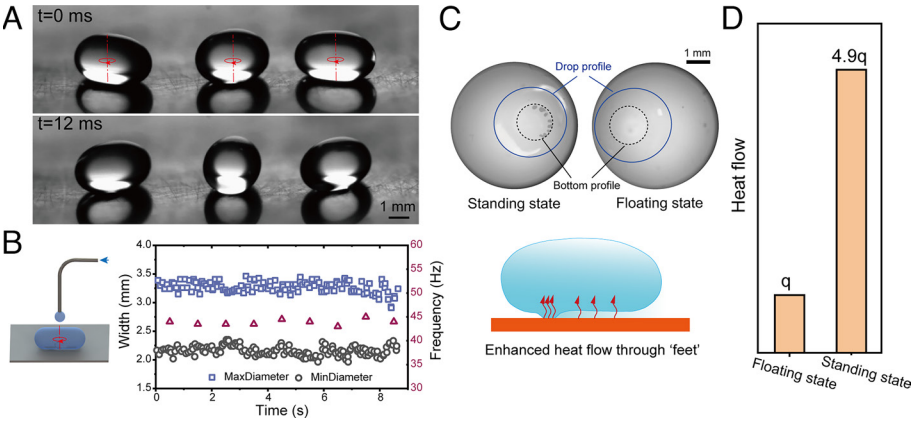

Fig. 4. Control of drop motion and enhanced heat-transfer efficiency in the standing Leidenfrost state. (*A*) Standing Leidenfrost drops and rotations observed on a silicon wafer with PDMS patterns. (*B*) Schematic illustration of the continuous water-feeding system for sustained rotation and the drop size and frequency as a function of time during rotation. (*C*) Images extracted from the standing and floating Leidenfrost states showing a distinct interaction between the drop and the surface. The schematic illustration shows the enhanced heat transfer through adhesion in the standing Leidenfrost state. (*D*) Enhancement of heat flow of 390% between the substrate and the drop in the standing state with partial adhesion (15%) compared with that in the floating state with a full insulating vapor layer.

drives the deformation and rotation of the drop and the control of the partial adhesion and rotation.

Materials and Methods

Materials. Sapphire slides with a diameter of 30 mm and a thickness of 2 mm were purchased from ALFAQUARTZ Products Co., Ltd. An oxidized silicon wafer (500-μm-thick Si layer with a 1-μm-thick SiO_2 top layer) was purchased from Suzhou Research Materials Microtech Co., Ltd. Ultrapure water was used in all experiments and was supplied by a Milli-Q Advantage A10 device (Millipore). Poly(dimethylsiloxane) terminated with chlorine (PDMS-Cl; average M_n of ~3,000 and 1H,1H,2H,2H-perfluorooctyl-trichlorosilane (97% pure) was acquired from Sigma-Aldrich. The photoresist (AZnLOF 2035) was from MicroChemicals GmbH. A fluorescent tracer (polystyrene, 5 μm in diameter) was purchased from PHOSPHOREX, LLC. Poly(dimethylsiloxane) with Sylgard 184 elastomer (PDMS) was purchased from Dow Corning.

Preparation of Chemically and Topologically Homogeneous Slides. Before use, the bare sapphire slides were cleaned with piranha solution to remove any organic contaminants. The sapphire glass was then activated by O_2 plasma for 15 min to graft the PDMS-Cl molecules and 1H,1H,2H,2H-perfluorooctyl-trichlorosilane onto the surface. The plasma-cleaned slides were placed in a desiccator along with 200 μL of the solutions and placed under vacuum at a pressure of ~100 mbar. The desiccator was then placed in an oven for 2 h at 60 °C and room temperature for grafting PDMS-Cl molecules and 1H,1H,2H,2H-perfluorooctyl-trichlorosilane, respectively.

Surface Characterization. Surface wetting was characterized using the sessile-drop method with an OCA 50 AF (DataPhysics) instrument. The apparent water contact angle and contact-angle hysteresis (sliding angle) were determined using drop volumes of 5 and 10 μL, respectively. During the measurement of contact-angle hysteresis, the rate of the tilting angle was set at 1°/s. The surface morphology was scanned using AFM (Bioscope Resolve, Bruker, USA) in peak-force mode (PeakForce Quantitative NanoMechanics) with an SNL-A probe. All data were obtained from the measurements of three different samples, with at least three different locations for each sample.

Visualization of the Standing Leidenfrost Drop. The temperature of the sample substrate was controlled using a heating stage. Specifically, the sample substrate was placed on a heater with a central hole (20-mm diameter) for visualization from the bottom. For each experiment, the temperature of the heating stage was kept constant, with an accuracy of 0.1 °C. The sample substrate required less than 1 min to achieve a uniformly distributed temperature across its surface. The drop was captured using a high-speed camera (Photron, Fastcam SA5) from the top, bottom, and side. The frame rate ranged from 500 to 2,000 fps, depending on the motion of the drop. An infrared camera (Fortic, 226s) was used to visualize the surface-temperature distribution from the bottom at 25 fps. The probability of standing Leidenfrost state on smooth hydrophobic sapphire slides was determined by imaging the contact area. The volume of the drops ranged from 3 to 40 μL, and the temperature ranged from 160 to 190 °C. The probability of ellipsoidal rotation was determined by analyzing several drops positioned on micropatterned surfaces with asymmetric effusivity. The volume of the drops ranged from 5 to 65 μL, and the temperature ranged from 170 to 280 °C. To ensure statistical significance, the probability was measured for a minimum of 10 drops.

Visualization of the Inner Flow Field. The internal flows were visualized using a custom-built PIV system. A fluorescent tracer was dispersed in water and diluted by a factor of 50. The surface tension of the drop was reduced to approximately 30 mN/s by adding the tracer. The solution was sonicated for 10 min to achieve thorough mixing before use. To illuminate the particles, a light sheet with a thickness of 50 μm at a wavelength of 532 nm was generated using a laser (Changchun New Industries Optoelectronics Tech. Co., Ltd., MGL-F-532-3W). Images captured at a speed of 2,000 fps were analyzed using PIVlab software to determine the velocity field inside the drop.

Fabrication of Micropatterned Surfaces with Asymmetric Effusivity. Micropatterned surfaces were fabricated using photolithography, followed by deep reactive ion etching (DRIE). First, a 1.9-μm-thick layer of photoresist AZnLOF 2035 (MicroChemicals, GmbH) was spin-coated on an oxidized silicon wafer (500-μm-thick Si layer with a 1-μm-thick SiO_2 top layer). The micropattern was designed with AutoCAD software and lithographed to the photoresist film using a uPG501 UV-light mask writer (Heidelberg Instruments) to obtain a soft mask after development and baking. To transfer the micropattern to the SiO_2 film, anisotropic SiO_2 DRIE (Oxford Instruments, PlasmaPro 100 Estrelas) was used, followed by ultrasonic cleaning in acetone to remove the remaining photoresist. This SiO_2 pattern was used as a hard mask to achieve 50-μm-deep etching using a 255-loop DRIE Bosch process. The surface was filled with PDMS after final oxygen plasma cleaning to remove the passivation layer and was placed in a buffered-oxide-etch bath to remove the remaining SiO_2. The PDMS was prepared by mixing the base component and a cross-linker at a ratio of 10:1 by weight. After manual stirring for 2 min, the solution was degassed under vacuum for 15 min. The degassed solution was poured on the micropatterned wafer until all the patterns were filled. The sample was then cured in an oven at 60 °C for 2 h. The excess PDMS on the surface was removed with a sharp knife.

Data, Materials, and Software Availability. All study data are included in the article and/or supporting information.

ACKNOWLEDGMENTS. We acknowledge funding support by the National Natural Science Foundation of China (22072014, 22102017, 52103136, and 52106194), the Sichuan Outstanding Young Scholars Foundation (2021JDJQ0013), the Sichuan Science and Technology Program (2021JDRC0016 and 2023JDRC0082), and Project of Key Laboratory of Intelligent Processing Technology for Digital Music (Zhejiang Conservatory of Music), Ministry of Culture and Tourism (2022DMKLC005).

1. P. Agrawal, G. McHale, Leidenfrost effect and surface wettability in *The Surface Wettability Effect on Phase Change*, M. Marengo, J. De Coninck, Eds. (Springer International Publishing, Cham, 2022), pp. 189–233.
2. H. Jo, H. S. Ahn, S. Kang, M. H. Kim, A study of nucleate boiling heat transfer on hydrophilic, hydrophobic and heterogeneous wetting surfaces. *Int. J. Heat Mass Transf.* **54**, 5643–5652 (2011).
3. Y. Song, L. Zhang, C. D. Díaz-Marín, S. S. Cruz, E. N. Wang, Unified descriptor for enhanced critical heat flux during pool boiling of hemi-wicking surfaces. *Int. J. Heat Mass Transf.* **183**, 122189 (2022).
4. H. J. Cho, D. J. Preston, Y. Zhu, E. N. Wang, Nanoengineered materials for liquid–vapour phase-change heat transfer. *Nat. Rev. Mater.* **2**, 16092 (2016).
5. S. Lyu *et al.*, On explosive boiling of a multicomponent Leidenfrost drop. *Proc. Natl. Acad. Sci. U.S.A.* **118**, e2016107118 (2021).
6. J. G. Leidenfrost, *De Aquae Communis Nonnullis Qualitatibus Tractatus* (Ovenius, 1756).
7. D. Quéré, Leidenfrost dynamics. *Annu. Rev. Fluid Mech.* **45**, 197–215 (2013).
8. T. Y. Zhao, N. A. Patankar, The thermo-wetting instability driving Leidenfrost film collapse. *Proc. Natl. Acad. Sci. U.S.A.* **117**, 13321–13328 (2020).
9. A. Bouillant, C. Cohen, C. Clanet, D. Quéré, Self-excitation of Leidenfrost drops and consequences on their stability. *Proc. Natl. Acad. Sci. U.S.A.* **118**, e2021691118 (2021).
10. X. Ma, J. C. Burton, Self-organized oscillations of Leidenfrost drops. *J. Fluid Mech.* **846**, 263–291 (2018).
11. G. Paul, P. K. Das, I. Manna, Droplet oscillation and pattern formation during Leidenfrost phenomenon. *Exp. Therm. Fluid Sci.* **60**, 346–353 (2015).
12. A. Bouillant *et al.*, Leidenfrost wheels. *Nat. Phys.* **14**, 1188–1192 (2018).
13. H. Linke *et al.*, Self-propelled leidenfrost droplets. *Phys. Rev. Lett.* **96**, 154502 (2006).
14. C. Liu, C. Lu, Z. Yuan, C. Lv, Y. Liu, Steerable drops on heated concentric microgroove arrays. *Nat. Commun.* **13**, 3141 (2022).
15. J. Li *et al.*, Directional transport of high-temperature Janus droplets mediated by structural topography. *Nat. Phys.* **12**, 606–612 (2016).
16. A. Gauthier, C. Diddens, R. Proville, D. Lohse, D. van der Meer, Self-propulsion of inverse Leidenfrost drops on a cryogenic bath. *Proc. Natl. Acad. Sci. U.S.A.* **116**, 1174–1179 (2019).
17. G. Graeber *et al.*, Leidenfrost droplet trampolining. *Nat. Commun.* **12**, 1727 (2021).
18. S. Lyu *et al.*, Final fate of a leidenfrost droplet: Explosion or takeoff. *Sci. Adv.* **5**, eaav8081 (2019).
19. S. R. Waitukaitis, A. Zuiderwijk, A. Souslov, C. Coulais, M. van Hecke, Coupling the leidenfrost effect and elastic deformations to power sustained bouncing. *Nat. Phys.* **13**, 1095–1099 (2017).
20. J. de Ruiter, R. Lagraauw, D. van den Ende, F. Mugele, Wettability-independent bouncing on flat surfaces mediated by thin air films. *Nat. Phys.* **11**, 48–53 (2015).
21. J. T. Pham *et al.*, Spontaneous jumping, bouncing and trampolining of hydrogel drops on a heated plate. *Nat. Commun.* **8**, 905 (2017).
22. H. Teisala, P. Baumli, S. A. L. Weber, D. Vollmer, H.-J. Butt, Grafting silicone at room temperature–a transparent, scratch-resistant nonstick molecular coating. *Langmuir* **36**, 4416–4431 (2020).
23. J. Burton, A. Sharpe, R. Van Der Veen, A. Franco, S. Nagel, Geometry of the vapor layer under a Leidenfrost drop. *Phys. Rev. Lett.* **109**, 074301 (2012).
24. E. Yim, A. Bouillant, F. Gallaire, Buoyancy-driven convection of droplets on hot nonwetting surfaces. *Phys. Rev. E* **103**, 053105 (2021).
25. W. Thielicke, R. Sonntag, Particle image velocimetry for MATLAB: Accuracy and enhanced algorithms in PIVlab. *J. Open Res. Softw.* **9**, 1–13 (2021).

26. R. Hill, L. Eaves, Nonaxisymmetric shapes of a magnetically levitated and spinning water droplet. *Phys. Rev. Lett.* **101**, 234501 (2008).
27. S. Chandrasekhar, The stability of a rotating liquid drop. *Proc. R. Soc. Lond. A Math. Phys. Sci.* **286**, 1–26 (1965).
28. T. Wang, E. Trinh, A. Croonquist, D. Elleman, Shapes of rotating free drops: Spacelab experimental results. *Phys. Rev. Lett.* **56**, 452 (1986).
29. J. A. F. Plateau, *Annual Report of the Board of Regents of the Smithsonian Institution* (The Smithsonian Institution, Washington DC, 1863).
30. P. Aussillous, D. Quéré, Shapes of rolling liquid drops. *J. Fluid Mech.* **512**, 133–151 (2004).
31. R. Brown, L. Scriven, The shape and stability of rotating liquid drops. *Proc. R. Soc. Lond. A Math. Phys. Sci.* **371**, 331–357 (1980).
32. E. Yim, A. Bouillant, D. Quéré, F. Gallaire, Leidenfrost flows: Instabilities and symmetry breakings. *Flow* **2**, E18 (2022).
33. E. Bormashenko, Motion of the liquid on the surface of leidenfrost droplets and the hairy ball theorem. *Surf. Innov.* **7**, 101–103 (2019).
34. M. A. J. van Limbeek *et al.*, Leidenfrost drops cooling surfaces: Theory and interferometric measurement. *J. Fluid Mech.* **827**, 614–639 (2017).
35. J. A. Balderas-Lopez *et al.*, Photoacoustic measurements of transparent liquid samples: Thermal effusivity. *Meas. Sci. Technol.* **6**, 1163 (1995).
36. J. Wang, R. Bras, G. Sivandran, R. Knox, A simple method for the estimation of thermal inertia. *Geophys. Res. Lett.* **37**, L05404 (2010).
37. H.-J. Butt, K. Graf, M. Kappl, *Physics and Chemistry of Interfaces* (John Wiley & Sons, 2023).